# Multipoint Inverse Airfoil Design Method Based on Conformal Mapping

Michael S. Selig* and Mark D. Maughmer†

*Pennsylvania State University, University Park, Pennsylvania 16802*

A method of multipoint inverse airfoil design for incompressible potential flow is presented. Multipoint design is handled by dividing the airfoil into a number of desired segments. For each segment, the velocity distribution is prescribed together with an angle of attack at which the prescribed velocity distribution is to be achieved. In this manner, multipoint design objectives can be taken into account in the initial specification of the velocity distribution. In order for the multipoint inverse airfoil design problem to be well posed, three integral constraints and several conditions arise that must be satisfied. Further restrictions are imposed if the airfoil is to have a specified pitching moment, thickness ratio, or other constraints. The system of equations is solved partly as a linear system and partly through multidimensional Newton iteration. Since the velocity distribution is prescribed about the circle in terms of the arc limit, specification of the velocity in terms of arc length is also handled through multidimensional Newton iteration.

## Nomenclature

$a_m, b_m$ = Fourier series coefficients
$c$ = airfoil chord
$c_{m_0}$ = zero-lift pitching moment coefficient
$F(z)$ = complex potential function
$g(\phi), h(\phi)$ = positive, nonzero functions
$K$ = main-recovery parameter
$K_H$ = closure-recovery parameter
$K_S$ = trailing-edge thickness parameter
$P(\phi)$ = harmonic function on circle
$P_U(\phi)$ = smooth part of $P(\phi)$
$P_V(\phi)$ = part of $P(\phi)$ with sharp corners
$Q(\phi)$ = conjugate harmonic function on circle
$s$ = arc length about airfoil
$s_i$ = arc length for segment $i$
$\tilde{s}_i$ = relative arc length for segment $i$
$t/c$ = thickness ratio of airfoil
$v$ = velocity distribution on airfoil
$v_i$ = velocity level for segment $i$
$v_\alpha^*(\phi)$ = single-point design velocity distribution
$v_0^*(\phi)$ = single-point design velocity distribution at zero lift
$v^*(\phi)$ = multipoint design velocity distribution
$\tilde{v}_i(\tilde{\phi}_i)$ = relative design velocity distribution in terms of the arc limit for segment $i$
$\tilde{v}_i(\tilde{s}_i)$ = relative design velocity distribution in terms of the arc length for segment $i$
$w(\phi)$ = total recovery function
$w_F(\phi)$ = trailing-edge recovery function
$w_S(\phi)$ = closure-recovery function
$w_W(\phi)$ = main-recovery function
$z$ = physical-plane complex coordinate $(x + iy)$
$\alpha$ = angle of attack from zero-lift angle
$\alpha^*(\phi)$ = multipoint design angle-of-attack distribution
$\beta$ = stagnation point arc limit on circle
$\Gamma$ = circulation
$\Delta$ = denotes an increment

$\epsilon$ = trailing-edge included angle parameter
$\zeta$ = circle-plane complex coordinate $(\xi + i\eta)$
$\theta(\phi)$ = surface angle about airfoil
$\theta^*(\phi)$ = flow direction about airfoil
$\mu$ = main-recovery parameter
$\pi^*(\phi)$ = step function
$\phi$ = arc limit in circle plane
$\phi_i$ = arc limit for segment $i$
$\phi_F$ = trailing-edge recovery arc limit
$\phi_S$ = closure-recovery arc limit
$\phi_W$ = main-recovery arc limit
$\tilde{\phi}_i$ = relative arc limit for segment $i$

Subscripts

$+$ = from positive side
$-$ = from negative side

Superscripts

$\sim$ = relative to beginning of segment
$-$ = lower-surface quantity

## Introduction

O F particular importance in designing a new airfoil is the ability to achieve the desired airfoil performance at more than one operating condition. For example, requirements are typically placed on the maximum and minimum lift coefficients, the width of the low-drag range, airfoil thickness ratio, and pitching moment, just to name a few. The particular performance characteristics required at the various operating conditions can most easily be obtained through the use of a method that allows for multipoint design. Airfoil optimization formulations can allow for multipoint design, but the suitable object function is difficult to define and computational requirements are demanding.

Several single-point inverse airfoil design methods make use of the Lighthill integral constraints, which guarantee uniform flow at infinity and closure of the airfoil profile.[1-7] Each of these methods requires as input the velocity distribution (subject to the integral constraints) at one angle of attack, typically that at zero lift. Whether the airfoil satisfies the multipoint design requirements is determined through postdesign analysis at the operating conditions of interest. Although multipoint airfoil design via this scheme has lead to many successful airfoils, a method that has the explicit capability of handling multipoint design requirements is favored since it is more direct and demands less computation time.

The theory of Eppler,[8-10] which uses conformal mapping, has multipoint design capability. A distinction is made between this theory, which is quite general, and the specific solution formulation. This method has been made readily available as a computer program.[9-11] Airfoils designed via this program can be found throughout the literature, and actual applications are numerous. Paradoxically, despite the versatility of the method, the theory itself has not received a great deal of attention since its original presentation in 1957.

As will be discussed and illustrated later, the Eppler method allows the designer to divide the airfoil into segments along each of which the velocity is prescribed to be constant at a specified angle of attack relative to zero lift. In this way, multipoint design objectives can be satisfied during the actual design effort as opposed to designing by a single-point method and examining afterwards multipoint design objectives.

This paper presents a new solution and extension of the Eppler theory, whereby the designer has greater flexibility during the design process. The velocity distribution along each airfoil segment may be a prescribed function, not necessarily constant. In addition to having control over the trailing-edge thickness distribution, as in the Eppler method, the airfoil may be designed to have either a cusped or finite trailing-edge angle. This is made possible by assuming a more general form of the mapping function. Also, if desired, the airfoil thickness, pitching moment, and other important design parameters may be specified, and the velocity distribution in terms of arc length may be prescribed. This increased generality is achieved first by formulating the solution in a new way and, second, by employing a multidimensional Newton iteration procedure to solve the resulting nonlinear system of equations.

## Theoretical Background

In what follows, the derivation of the equations for the multipoint inverse airfoil design is presented along lines similar to those given by Eppler.[8] The essential difference being that Eppler's derivation is for cusped airfoils, whereas here cusped and finite trailing-edge angle airfoils are considered.

The complex potential for uniform flow of unit velocity at angle of attack $\alpha$ about a unit circle in the $\zeta$ plane is given by

$$F(\zeta) = e^{-i\alpha}\zeta + \frac{e^{i\alpha}}{\zeta} + \frac{i\Gamma}{2\pi}\ln\zeta \qquad (1)$$

where $\Gamma = 4\pi\sin\alpha$ is required to satisfy the Kutta condition by fixing the rear stagnation point at $\zeta = 1$. The front stagnation point is then located at $\phi = \pi + 2\alpha$. To obtain the flow about an arbitrary airfoil in the $z$ plane, the flow about the circle in the $\zeta$ plane is mapped via $z = z(\zeta)$, as illustrated in Fig. 1.
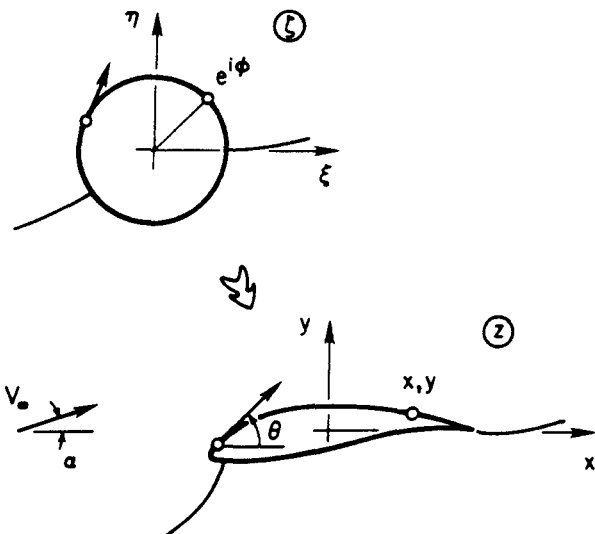


**Fig. 1  Mapping from circle to airfoil plane.**

The mapping must satisfy three conditions: the airfoil trailing-edge angle must be finite, the flow at infinity must be unaltered, and the airfoil contour must close. These latter two conditions ultimately lead to the integral constraints for multipoint inverse airfoil design. The transformation is assumed to be of the form

$$\frac{dz}{d\zeta} = \left(1 - \frac{1}{\zeta}\right)^{1-\epsilon} e^{\sum_{m=0}^{\infty}(a_m + ib_m)\zeta^{-m}}, \qquad |\zeta| \geq 1 \qquad (2)$$

As discussed by James,[12] the factor $(1 - 1/\zeta)^{1-\epsilon}$ guarantees an airfoil with a trailing-edge angle of $\pi\epsilon$. Taking $\epsilon = 0$ for cusped airfoil yields the transformation used by Eppler.[8] To determine the remaining conditions on the mapping, it is helpful to expand Eq. (2) as

$$\frac{dz}{d\zeta} = e^{a_0 + ib_0}\left[1 + \frac{a_1 - 1 + \epsilon + ib_1}{\zeta} + \mathcal{O}\left(\frac{1}{\zeta^2}\right)\right], \qquad |\zeta| \geq 1 \qquad (3)$$

The condition that the flow at infinity be unaltered is expressed as

$$\lim_{\zeta \to \infty} \frac{dz}{d\zeta} = 1 \qquad (4)$$

which is only satisfied if

$$a_0 = 0, \qquad b_0 = 0 \qquad (5)$$

The condition that the airfoil be closed can be written as

$$\oint dz = \oint \frac{dz}{d\zeta}d\zeta = 0 \qquad (6)$$

which is only satisfied if

$$a_1 = 1 - \epsilon, \qquad b_1 = 0 \qquad (7)$$

The problem at hand is to relate the desired velocity distribution about the airfoil to the series coefficients of the mapping. To this end, the complex velocity in the $z$ plane is expressed as

$$\frac{dF}{dz} = ve^{-i\theta} \qquad (8)$$

which on the boundary of the unit circle, $\zeta = e^{i\phi}$, becomes

$$\left(\frac{dF}{dz}\right)_{e^{i\phi}} = v(\phi)e^{-i\theta(\phi)} \qquad (9)$$

Obtaining the real and imaginary parts of Eq. (9) for later use is facilitated by taking its natural logarithm. This, however, requires special consideration since $v(\phi)$ is negative along the lower surface aft of the leading-edge stagnation point, as shown in Fig. 2. This problem is alleviated by taking the absolute value, $|v(\phi)| = v^*(\phi)$. In so doing, the flow direction must jump by $\pi$ at the leading-edge stagnation point and by $\pi\epsilon$ at the trailing edge. To reflect these jumps, $\theta(\phi)$ is replaced by $\theta^*(\phi)$. Now

$$\left(\frac{dF}{dz}\right)_{e^{i\phi}} = v^*(\phi)e^{-i\theta^*(\phi)} \qquad (10)$$



**Fig. 2  Relation between $v(\phi)$ and $v^*(\phi)$.**

and taking the natural logarithm yields

$$\ell n \left(\frac{dF}{dz}\right)_{e^{i\phi}} = \ell n \, v^*(\phi) - i\,\theta^*(\phi) \tag{11}$$

To relate $v^*(\phi)$ and $\theta^*(\phi)$ to the series coefficients, the complex velocity is written alternatively as

$$\left(\frac{dF}{dz}\right)_{e^{i\phi}} = \frac{(dF/d\zeta)_{e^{i\phi}}}{(dz/d\zeta)_{e^{i\phi}}} \tag{12}$$

The numerator $(dF/d\zeta)_{e^{i\phi}}$ is simply the known flow over the circle given by

$$\left(\frac{dF}{d\zeta}\right)_{e^{i\phi}} = 4\sin\frac{\phi}{2}\cos\left[\frac{\phi}{2}-\alpha^*(\phi)\right]e^{-i(\phi-\pi/2)} \tag{13}$$

The reason for writing the angle of attack as $\alpha^*(\phi)$ will be explained later. Since the factor $\cos[\phi/2-\alpha^*(\phi)]$ is negative for $\pi+2\alpha^*(\phi)<\phi<2\pi$, the complex velocity about the circle is, in preparation for taking its natural logarithm, alternatively written as

$$\left(\frac{dF}{d\zeta}\right)_{e^{i\phi}} =$$

$$4\sin\frac{\phi}{2}\left|\cos\left[\frac{\phi}{2}-\alpha^*(\phi)\right]\right|\left|\exp\left\{-i\left[\phi-\pi/2-\pi^*(\phi)\right]\right\}\right. \tag{14}$$

where

$$\pi^*(\phi) = \begin{cases} 0, & 0\le\phi\le\pi+2\alpha^*(\phi) \\ \pi, & \pi+2\alpha^*(\phi)\le\phi\le2\pi \end{cases} \tag{15}$$

The step function $\pi^*(\phi)$ is introduced in order to account properly for the jumps in the flow direction at the front and rear stagnation points on the circle.

From Eq. (2), the derivative of the mapping function on the unit circle is

$$\left(\frac{dz}{d\zeta}\right)_{e^{i\phi}} = (1-e^{-i\phi})^{1-\epsilon}\exp\sum_{m=0}^{\infty}(a_m+ib_m)e^{-im\phi} \tag{16}$$

or

$$\left(\frac{dz}{d\zeta}\right)_{e^{i\phi}} = (1-e^{-i\phi})^{1-\epsilon}e^{P(\phi)+iQ(\phi)} \tag{17}$$

where

$$P(\phi)+iQ(\phi) = \sum_{m=0}^{\infty}(a_m\cos m\phi+b_m\sin m\phi)$$

$$+ i\sum_{m=0}^{\infty}(b_m\cos m\phi-a_m\sin m\phi) \tag{18}$$

Using expressions (14) and (17) and taking the natural logarithm of Eq. (12), the following result is ultimately obtained

$$\ell n\left(\frac{dF}{dz}\right)_{e^{i\phi}} = -\ell n\left\{\frac{(2\sin\phi/2)^{-\epsilon}}{2|\cos[\phi/2-\alpha^*(\phi)]|}\right\}$$

$$+ i\left\{\pi^*(\phi)-\frac{\phi}{2}+\epsilon\left(\frac{\pi}{2}-\frac{\phi}{2}\right)\right\} - P(\phi) - iQ(\phi) \tag{19}$$

Equating Eqs. (11) and (19) gives the important result

$$P(\phi)+iQ(\phi) = -\ell n\left\{\frac{(2\sin\phi/2)^{-\epsilon}v^*(\phi)}{2|\cos[\phi/2-\alpha^*(\phi)]|}\right\}$$

$$+ i\left\{\theta^*(\phi)+\pi^*(\phi)-\frac{\phi}{2}+\epsilon\left(\frac{\pi}{2}-\frac{\phi}{2}\right)\right\} \tag{20}$$

where $0\le\phi\le2\pi$.

It is seen from Eq. (20) that specifying the velocity $v^*(\phi)$ and angle of attack $\alpha^*(\phi)$ uniquely determines $P(\phi)$. Alternatively, specifying the airfoil flow direction $\theta^*(\phi)$ and $\alpha^*(\phi)$ uniquely determines $Q(\phi)$. From either $P(\phi)$ or $Q(\phi)$, the corresponding conjugate harmonic function may be determined through Poisson's integral exterior to the circle, that is,

$$P(\phi)+iQ(\phi) = -\frac{1}{2\pi}\int_0^{2\pi}Q(\psi)\cot\frac{\psi-\phi}{2}\,d\psi$$

$$+ i\frac{1}{2\pi}\int_0^{2\pi}P(\psi)\cot\frac{\psi-\phi}{2}\,d\psi \tag{21}$$

A discussion of how $Q(\phi)$ is determined numerically from $P(\phi)$ will come later.

Once $P(\phi)$ and $Q(\phi)$ are known, the airfoil coordinates may be computed by equating the expression

$$\left(\frac{dz}{d\zeta}\right)_{e^{i\phi}} = \frac{dz/d\phi}{d\zeta/d\phi} = -ie^{-i\phi}\left(\frac{dx}{d\phi}+i\frac{dy}{d\phi}\right) \tag{22}$$

with Eq. (17). After some manipulation, this gives

$$x(\phi)+iy(\phi) = -\int\left(2\sin\frac{\phi}{2}\right)^{1-\epsilon}$$

$$\times e^{P(\phi)}\exp\left\{i\left[\phi/2-\epsilon(\pi/2-\phi/2)+Q(\phi)\right]\right\}d\phi \tag{23}$$

The airfoil coordinates $x(\phi)$ and $y(\phi)$ are then obtained through quadrature.

## Multipoint Design Capability of the Theory

For discussion, $P(\phi)$ is rewritten as

$$P(\phi) = -\ell n\left\{\frac{(2\sin\phi/2)^{-\epsilon}v^*(\phi)}{2|\cos[\phi/2-\alpha^*(\phi)]|}\right\} = f(\phi) \tag{24}$$

The function $P(\phi)$ depends only on $\phi$ and is defined by specification of $v^*(\phi)$ and $\alpha^*(\phi)$, now termed the design velocity distribution and the corresponding design angle-of-attack distribution. For single-point design, as in Lighthill's theory,[1] $\alpha^*(\phi)$ is zero, whereas $v^*(\phi)$ is a continuous specified function. It is not necessary, however, that $v^*(\phi)$ and $\alpha^*(\phi)$ be continuous functions; rather, it is only necessary that $P(\phi)$ be continuous. This continuity of $P(\phi)$ is analogous to prescribing a continuous velocity distribution for the airfoil at a single angle of attack. Therefore, in order to maintain a continuous function $P(\phi)$, a discontinuity in $v^*(\phi)$ between two segments must be compensated by a corresponding discontinuity in $\alpha^*(\phi)$. Consequently, the airfoil may be divided into any number of segments along which the velocity $v^*(\phi)$ and angle of attack $\alpha^*(\phi)$ are given. Practical considerations for multipoint design dictate that over each segment $\alpha^*(\phi)$ be constant, whereas $v^*(\phi)$ may vary in order to obtain some desired velocity distribution over the given segment at the design angle of attack $\alpha^*(\phi)$. This process of specifying $v^*(\phi)$ for different segments of the airfoil at different angles of attack $\alpha^*(\phi)$ easily allows for multipoint design. This is the most important result of the theory: discrete segments of the airfoil may be designed for different angles of attack or, more generally, each segment may be designed for a different operating condition (Reynolds number, angle of attack, etc.). This result will be illustrated later by example.

## Integral Constraints for Inverse Airfoil Design

As with any inverse airfoil design formulation, the specification of the velocity distribution is not completely arbitrary. Since the function $P(\phi)$ can be expressed as a Fourier series with $Q(\phi)$ being its conjugate series, the constraints on the mapping coefficients, Eqs. (5) and (7), give rise to integral

constraints on both $P(\phi)$ and $Q(\phi)$. The integral constraints on $P(\phi)$ come from the first three coefficients of the Fourier series representation for $P(\phi)$, that is, from Eqs. (18), (5), and (7)

$$a_0 = \frac{1}{2\pi} \int_0^{2\pi} P(\phi)\, d\phi = 0 \tag{25a}$$

$$a_1 = \frac{1}{\pi} \int_0^{2\pi} P(\phi)\cos\phi\, d\phi = 1 - \epsilon \tag{25b}$$

$$b_1 = \frac{1}{\pi} \int_0^{2\pi} P(\phi)\sin\phi\, d\phi = 0 \tag{25c}$$

Likewise, the three integral constraints on $Q(\phi)$ are

$$b_0 = \frac{1}{2\pi} \int_0^{2\pi} Q(\phi)\, d\phi = 0 \tag{26a}$$

$$b_1 = \frac{1}{\pi} \int_0^{2\pi} Q(\phi)\cos\phi\, d\phi = 0 \tag{26b}$$

$$-a_1 = \frac{1}{\pi} \int_0^{2\pi} Q(\phi)\sin\phi\, d\phi = \epsilon - 1 \tag{26c}$$

Considering the expressions for $P(\phi)$ and $Q(\phi)$, it is seen that Eqs. (25) are integral constraints on $v^*(\phi)$ and $\alpha^*(\phi)$, whereas Eqs. (26) are integral constraints on $\theta^*(\phi)$ and $\alpha^*(\phi)$.

As could be anticipated, the preceding integral constraints are closely related to several others found in the literature. In fact, they are thought to be the most general form of the integral constraints for incompressible inverse airfoil design. For cusped airfoils, the integral constraints on $P(\phi)$ are equivalent to those of Eppler[8] when $\epsilon = 0$. For single-point design in which the angle of attack $\alpha$ is constant, the integral constraints reduce to those of Strand[7] given for $\ell_n v_\alpha^*(\phi)$ and $\theta_\alpha^*(\phi)$ by

$$\int_0^{2\pi} \ell_n v_\alpha^*(\phi) \begin{Bmatrix} 1 \\ \cos\phi \\ \sin\phi \end{Bmatrix} d\phi = \begin{Bmatrix} 0 \\ -2\pi \sin^2\alpha \\ \pi \sin2\alpha \end{Bmatrix} \tag{27a}$$

$$\int_0^{2\pi} \theta_\alpha^*(\phi) \begin{Bmatrix} 1 \\ \cos\phi \\ \sin\phi \end{Bmatrix} d\phi = \begin{Bmatrix} 2\pi\alpha \\ -\pi \sin2\alpha \\ -2\pi \sin^2\alpha \end{Bmatrix} \tag{27b}$$

For single-point design at zero lift where $\alpha^*(\phi) = 0$ and $\ell_n v^*(\phi) = \ell_n v_0^*(\phi)$, the integral constraints on $P(\phi)$ reduce to

$$\int_0^{2\pi} \ell_n v_0^*(\phi) \begin{Bmatrix} 1 \\ \cos\phi \\ \sin\phi \end{Bmatrix} d\phi = \begin{Bmatrix} 0 \\ 0 \\ 0 \end{Bmatrix} \tag{28}$$

as presented by Lighthill.[1] It is not well known that these last integral constraints commonly attributed to Lighthill were derived earlier by Mangler.[13] Furthermore, as noted by Mangler, essentially the same conditions were found even earlier by Betz[14] and, for the most part, by Weinig.[15]

### Continuity Constraints

For multipoint design, the requirement that $P(\phi)$ be continuous introduces a *continuity* equation on $P(\phi)$ at each arc limit between segments where there is a jump in $v^*(\phi)$ and a corre-

sponding jump in $\alpha^*(\phi)$. This condition of continuity between segments is expressed as

$$P_+(\phi_i) = P_-(\phi_i) \tag{29a}$$

or

$$\frac{v_+^*(\phi_i)}{|\cos[\phi_i/2 - \alpha_+^*(\phi_i)]|} = \frac{v_-^*(\phi_i)}{|\cos[\phi_i/2 - \alpha_-^*(\phi_i)]|} \tag{29b}$$

where $\phi_i$ is the arc limit between segments $i$ and $i + 1$. This condition of continuity is not strictly necessary. For instance, the design velocity distribution could jump discontinuously at a point on a segment and thereby model suction[1,2] or blowing on the airfoil surface. Such airfoil flows will not be considered here, and $P(\phi)$ is required to be continuous as previously indicated.

### Leading- and Trailing-Edge Stagnation Point Velocity Laws

The velocity distribution must satisfy not only the integral constraints and continuity conditions, but in the vicinity of the stagnation points it must also follow a special law. This may be seen through Eq. (20), which gives

$$v^*(\phi) = (2 \sin\phi/2)^{\epsilon} 2|\cos[\phi/2 - \alpha^*(\phi)]| e^{-P(\phi)} \tag{30}$$

Stagnation points will always occur at the aerodynamic leading edge $\phi = \pi + 2\alpha^*(\phi)$ and, when $\epsilon \neq 0$, at the trailing edge $\phi = 0$, $\phi = 2\pi$. The velocity in the vicinity of the trailing edge must follow the general law

$$\lim_{\phi_+ \to 0} v^*(\phi) \sim (\sin\phi/2)^{\epsilon} g_+(\phi) \tag{31a}$$

$$\lim_{\phi_- \to 2\pi} v^*(\phi) \sim (\sin\phi/2)^{\epsilon} g_-(\phi) \tag{31b}$$

where $g_+(\phi)$ and $g_-(\phi)$ are positive, nonzero functions. James[12] obtained the same theoretical trailing-edge velocity law in an effort to understand the airfoil trailing-edge curvature singularity. Similarly, from Eq. (30), the velocity in the vicinity of the leading-edge stagnation point must follow

$$\lim_{\phi_- \to \beta} v_+^*(\phi) \sim |\cos[\phi/2 - \alpha^*(\phi)]| h_+(\phi) \tag{32a}$$

$$\lim_{\phi_- \to \beta} v_-^*(\phi) \sim |\cos[\phi/2 - \alpha^*(\phi)]| h_-(\phi) \tag{32b}$$

where the leading-edge stagnation point $\beta$ is at $\pi + 2\alpha^*(\phi)$ and where $h_+(\phi)$ and $h_-(\phi)$ are positive, nonzero functions.
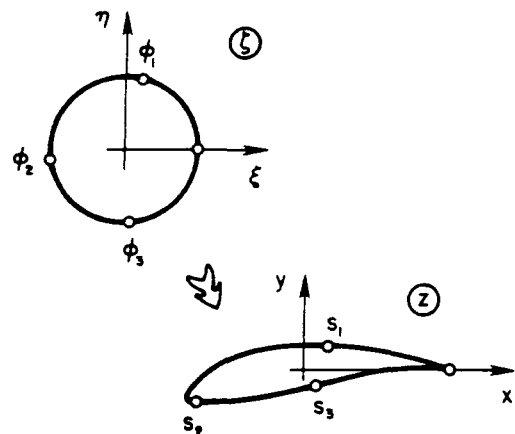


Fig. 3 Circle divided into four segments and mapped to an airfoil.

## Solution Formulation

The conditions on the mapping function that lead to the integral constraints on $P(\phi)$ require that the specification of $P(\phi)$ through $v^*(\phi)$ and $\alpha^*(\phi)$ must contain at least three free parameters to be determined by solution. For each segment, another free parameter must be introduced to satisfy the continuity constraint of $P(\phi)$ between segments. All of the necessary free parameters are introduced in a way to facilitate the numerical solution, to allow for implementation into the multidimensional Newton iteration, and to permit the design of practical airfoils.

### Specification of the Velocity Distribution

The four-segment airfoil depicted in Fig. 3 is given as an example. The design velocity distribution and the design angle-of-attack distribution for each segment are prescribed piecewise as follows:

$$v^*(\phi) = v_1 w(\phi)$$
$$\alpha^*(\phi) = \alpha_1, \qquad\qquad 0 \leq \phi \leq \phi_1 \qquad\qquad (33a)$$

$$v^*(\phi) = v_2 + \bar{v}_2(\tilde{\phi}_2)$$
$$\alpha^*(\phi) = \alpha_2, \qquad\qquad \phi_1 \leq \phi \leq \phi_2 \qquad\qquad (33b)$$

$$v^*(\phi) = v_3 + \bar{v}_3(\tilde{\phi}_3)$$
$$\alpha^*(\phi) = \alpha_3, \qquad\qquad \phi_2 \leq \phi \leq \phi_3 \qquad\qquad (33c)$$

$$v^*(\phi) = v_4 \bar{w}(\phi)$$
$$\alpha^*(\phi) = \alpha_4, \qquad\qquad \phi_3 \leq \phi \leq 2\pi \qquad\qquad (33d)$$

The velocities $v_i$ and the design angles of attack $\alpha_i$ are constant along their respective segments, whereas $\bar{v}_i(\tilde{\phi}_i)$, $w(\phi)$, and $\bar{w}(\phi)$ are functions. The velocity function $w(\phi)$ is termed the upper-surface recovery function, whereas $\bar{w}(\phi)$ is the corresponding function for the lower surface. The special notation ( ˜ ) will be discussed later. Although only four segments are presented here, the method can handle any number of intermediate segments of the type $v^*(\phi) = v_i + \bar{v}_i(\tilde{\phi}_i)$.

The upper-surface recovery function is defined by

$$w(\phi) = w_{\bar{w}}^{\mu}(\phi) w_S^{K_H}(\phi) w_F^t(\phi), \qquad 0 \leq \phi \leq \phi_1 \qquad (34)$$

where

$$w_W(\phi) = 1 + K\left(\frac{\cos\phi - \cos\phi_W}{1 + \cos\phi_W}\right), \qquad 0 \leq \phi \leq \phi_W \quad (35a)$$

$$w_S(\phi) = \begin{cases} 1 - 0.36\left(\dfrac{\cos\phi - \cos\phi_S}{1 - \cos\phi_S}\right)^2, & 0 \leq \phi \leq \phi_S \\ 1, & \theta_S \leq \phi \leq \phi_W \end{cases} \qquad (35b)$$

$$w_F(\phi) = \begin{cases} \dfrac{\sin\phi/2}{\sin\phi_F/2}, & 0 \leq \phi \leq \phi_F \\ 1, & \phi_F \leq \phi \leq \phi_W \end{cases} \qquad (35c)$$

with $\phi_W \equiv \phi_1$. The lower-surface recovery function $\bar{w}(\phi)$ is of the same form except that $w_W(\phi)$, $w_S(\phi)$, $w_F(\phi)$, and the defining parameters $\mu$, $K_H$, $K$, $\phi_W$, $\phi_S$, and $\phi_F$ are replaced by $\bar{w}_W(\phi)$, $\bar{w}_S(\phi)$, $\bar{w}_F(\phi)$, $\bar{\mu}$, $\bar{K}_H$, $\bar{K}$, $\bar{\phi}_W \equiv \phi_3$, $\bar{\phi}_S$, and $\bar{\phi}_F$.

For a typical airfoil design, $\phi_W > \phi_S > \phi_F$; for instance, $\phi_W = 100$ deg, $\phi_S = 20$ deg, and $\phi_F = 10$ deg. The first two recovery functions $w_W(\phi)$ and $w_S(\phi)$ appear in the original Eppler formulation, a good discussion of which is presented in Refs. 9 and 10. Briefly, for the choice of recovery arc limits given, the first factor $w_{\bar{w}}^{\mu}(\phi)$ controls the main part of the

recovery. The second factor $w_S^{K_H}(\phi)$ controls to a great extent the shape of the airfoil near the trailing edge and, most important, the thickness distribution in the vicinity of the trailing edge. By selecting appropriate values of $\mu$ and $K_H$, a broad range of practical recovery velocity distributions can be specified. The last factor $w_F^t(\phi)$ is new and must be introduced to satisfy the necessary trailing-edge velocity laws of Eqs. (31).

The design velocity distribution for a segment that contains the leading-edge stagnation point must follow the velocity law of Eqs. (32). There is, however, an important difference between the leading- and trailing-edge stagnation points; namely, the former one moves with angle of attack. It is possible to take advantage of this fact. Adopting the approach of Eppler, the design angle of attack for each segment is selected so that the leading-edge stagnation point at the design angle of attack falls outside of the segment, either ahead or behind. Consequently, the leading-edge stagnation point is entirely avoided, and the need to use the leading-edge stagnation point velocity laws of Eqs. (32) is bypassed.

A nonconstant design velocity distribution over each intermediate segment is introduced through the velocity functions $\bar{v}_i(\tilde{\phi}_i)$. This capability is not considered in the Eppler solution formulation. The notation ( ˜ ) is used to indicate the value relative to the beginning of the segment $i$. Thus, as drawn in Fig. 4, $\tilde{\phi}_i$ is the local arc limit for the segment. Likewise, the velocity $\bar{v}_i(\tilde{\phi}_i)$ is the velocity relative to the beginning of the segment such that

$$\bar{v}_i(\tilde{\phi}_i = 0) = 0 \qquad\qquad (36)$$

as indicated in Fig. 4. In Eqs. (33), $v_i$ is the velocity at the beginning of an intermediate segment $i$. Appropriately, $v_i$ and $\bar{v}_i(\tilde{\phi}_i)$ are, respectively, termed the velocity level and the relative design velocity distribution for an intermediate segment $i$. Consistent with the approach of avoiding a leading-edge stagnation point on a segment, it is required that $v^*(\phi) > 0$ or

$$v^*(\phi) = v_i + \bar{v}_i(\tilde{\phi}_i) > 0 \qquad\qquad (37)$$

The relative design velocity functions $\bar{v}_i(\tilde{\phi}_i)$ may be piecewise linear, cubic spline, or analytic functions and thereby offer a great deal of freedom in the design and especially in the Newton iteration scheme discussed later.

### Governing Equations for the Inverse Problem

Substituting the expressions for $v^*(\phi)$ and $\alpha^*(\phi)$, Eqs. (33), into the three integral constraints on $P(\phi)$ leads to

$$a_{11}\mu + a_{12}\bar{\mu} + a_{13}K_H + a_{14}\bar{K}_H = b_1 \qquad (38a)$$

$$a_{21}\mu + a_{22}\bar{\mu} + a_{23}K_H + a_{24}\bar{K}_H = b_2 \qquad (38b)$$

$$a_{31}\mu + a_{32}\bar{\mu} + a_{33}K_H + a_{34}\bar{K}_H = b_3 \qquad (38c)$$

where many of the terms in the coefficients $a_{jk}$ and $b_j$ are integrals expressible in closed form.[8]
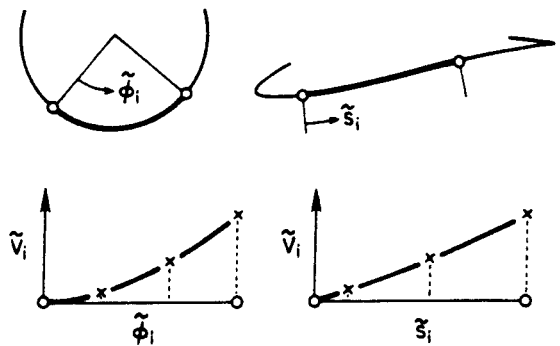


**Fig. 4   Relative design velocity on circle as mapped to an airfoil.**

It is of interest to note that the integral constraints on $P(\phi)$ are much easier to evaluate than those on $\ell_n v_\alpha^*(\phi)$, as done through Eqs. (27a) or (28) in Refs. 1-7. At the stagnation points, $\ell_n v_\alpha^*(\phi)$ is singular, whereas the singularities of $P(\phi)$ are removable owing to the velocity laws in the vicinity of the stagnation points. Hence, $P(\phi)$ is bounded in contrast to $\ell_n v_\alpha^*(\phi)$.

Continuity of $P(\phi)$ at the trailing edge gives

$$a_{41}\mu + a_{42}\bar{\mu} + a_{43}K_H + a_{44}\bar{K}_H = b_4 \tag{38d}$$

and, between the segments at $\phi_1$, $\phi_2$, and $\phi_3$, continuity further requires

$$\frac{v_2}{|\cos(\phi_1/2 - \alpha_2)|} = \frac{v_1}{|\cos(\phi_1/2 - \alpha_1)|} \tag{39a}$$

$$\frac{v_3}{|\cos(\phi_2/2 - \alpha_3)|} = \frac{v_2 + \tilde{v}_2(\tilde{\phi}_2 = \phi_2 - \phi_1)}{|\cos(\phi_2/2 - \alpha_2)|} \tag{39b}$$

$$\frac{v_4}{|\cos(\phi_3/2 - \alpha_4)|} = \frac{v_3 + \tilde{v}_3(\tilde{\phi}_3 = \phi_3 - \phi_2)}{|\cos(\phi_3/2 - \alpha_3)|} \tag{39c}$$

Table 1  Design variables for a four-segment airfoil

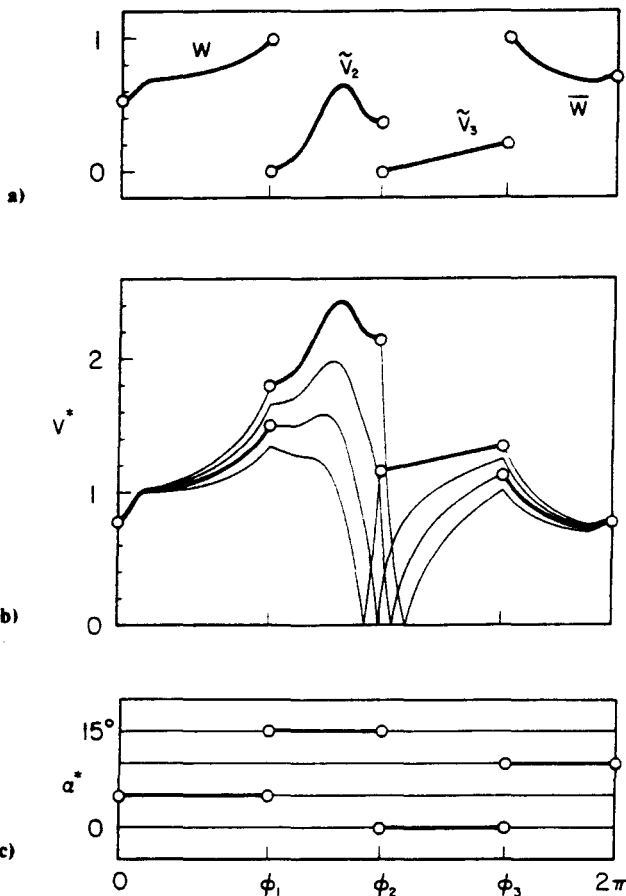| $i$ | $\phi$ | $\alpha^*(\phi)$ | $v^*(\phi)$ |
|---|---|---|---|
| 1 | $[0,\phi_1]$ | $\alpha_1$ | $v_1, w(\phi; \phi_W, \phi_S, \phi_F, K, \mu, K_H)$ |
| 2 | $[\phi_1,\phi_2]$ | $\alpha_2$ | $v_2, \tilde{v}_2(\tilde{\phi}_2)$ |
| 3 | $[\phi_2,\phi_3]$ | $\alpha_3$ | $v_3, \tilde{v}_3(\tilde{\phi}_3)$ |
| 4 | $[\phi_3,2\pi]$ | $\alpha_4$ | $v_4, \tilde{w}(\phi; \phi_W, \phi_S, \phi_F, K, \bar{\mu}, \bar{K}_H)$ |

a)

b)

c)

Fig. 5  Special velocity functions and design velocity and angle-of-attack distributions for a four-segment airfoil.
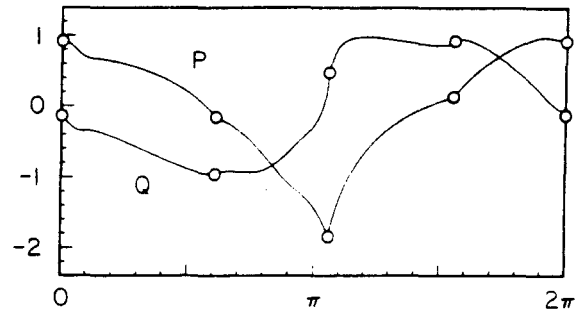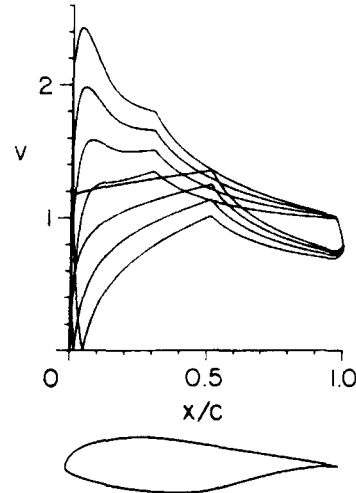
Fig. 6  Harmonic functions $P(\phi)$ and $Q(\phi)$.

Fig. 7  Airfoil and velocity distributions at $\alpha = 0$, 5, 10, and 15 deg.

Thus, there are seven equations to satisfy for an airfoil with four segments. Consequently, all but seven parameters can be specified.

Because of the convenient linearity of Eqs. (38) with respect to $\mu$, $\bar{\mu}$, $K_H$, and $\bar{K}_H$, it is natural to select these parameters as four of the required seven unknowns. Through the continuity equations (39), it is easiest to give any velocity level, say $v_1$, and from it compute the remaining velocity levels, $v_2$, $v_3$, and $v_4$. Therefore, a solution to the inverse airfoil problem can be determined by specifying all of the design variables except the seven that are unknown, $\mu$, $\bar{\mu}$, $K_H$, $\bar{K}_H$, $v_2$, $v_3$, and $v_4$. In summary, all of the design variables (besides $\epsilon$) for a four-segment airfoil are listed in Table 1.

## Application of the Theory

As an example of the method, a simple four-segment airfoil with a cusped trailing edge is presented. This airfoil and the others that follow are not intended for any practical application; rather, they merely serve as examples to illustrate the capabilities of the method. After specifying $\epsilon = 0$ to give a cusped trailing edge, together with everything listed in Table 1 except the seven unknowns, the system of Eqs. (38) and (39) can be solved. The solution yields $\mu$, $\bar{\mu}$, $K_H$, and $\bar{K}_H$, such that the recovery functions $w(\phi)$ and $\tilde{w}(\phi)$, plotted in Fig. 5a, are completely defined. Also shown in Fig. 5a are the prescribed relative velocity functions $\tilde{v}_2(\tilde{\phi}_2)$ and $\tilde{v}_3(\tilde{\phi}_3)$ satisfying the requirement that $\tilde{v}_i(\tilde{\phi}_i = 0) = 0$. The velocity function $\tilde{v}_2(\tilde{\phi}_2)$ is defined by a cubic spline of four points, and $\tilde{v}_3(\tilde{\phi}_3)$ is prescribed as linear. With $w(\phi)$, $\tilde{v}_2(\tilde{\phi}_2)$, $\tilde{v}_3(\tilde{\phi}_3)$, and $\tilde{w}(\phi)$ known and $v_2$, $v_3$, and $v_4$ found from the solution of the system, the complete design velocity distribution $v^*(\phi)$, shown in Fig. 5b, is obtained. Through Eq. (20), $\alpha^*(\phi)$ and $v^*(\phi)$ are used to form $P(\phi)$, which is plotted in Fig. 6. The jumps in $\alpha^*(\phi)$ that

are compensated by jumps in $v^*(\phi)$, such that $P(\phi)$ remains continuous, are seen in Figs. 5b, 5c, and 6. As determined using $P(\phi)$ through Poisson's integral, the conjugate harmonic function $Q(\phi)$ is also shown in Fig. 6. Airfoil coordinates are then computed using $P(\phi)$ and $Q(\phi)$. The airfoil profile together with the velocity distributions at $\alpha = 0, 5, 10$, and 15 deg are shown in Fig. 7.

To serve as a check on the numerical analysis and new code, it may be remarked that the velocity distributions for the airfoil shown in Fig. 7 are in close agreement with results from the high-order panel method analysis of Ref. 9.

### Numerical Evaluation of $Q(\phi)$

Some discussion on the calculation of $Q(\phi)$ from $P(\phi)$ is in order since this is the most difficult step in determining the airfoil. Many methods of solution exist in the literature, but the most suitable is that of Watson[16] and Garrick[17] and subsequently improved by Eppler[8] for the special circumstances of the present inverse formulation. As an overview, the method of Watson and Garrick involves first approximating the harmonic function by a truncated Fourier series. If the harmonic function is smooth, the fit is good; however, if the harmonic function has sharp corners, the fit about points near the sharp corners shows oscillations much like the Gibbs phenomenon. In Fig. 6, it is seen that $P(\phi)$ does have sharp corners between each segment with the one at $\phi_2$, near the airfoil leading edge, being the sharpest. Taking the approach of Eppler, the harmonic function $P(\phi)$ may be split into a smooth function and a part that contains the sharp corners, that is,

$$P(\phi) = P_U(\phi) + P_V(\phi) \qquad (40)$$

where $P_U(\phi)$ and $P_V(\phi)$ are the smooth part and the part with the sharp corners, respectively. Eppler only splits off the sharp corner at the leading-edge arc limit, but in the present method, all sharp corners are split off to improve the numerical accuracy. The split-off portion with the sharp corners $P_V(\phi)$ and its conjugate harmonic are expressed analytically,[8] whereas the conjugate harmonic to the smooth $P_U(\phi)$ is computed numerically according to Refs. 16 and 17. Eppler notes that this numerical step is equivalent to two fast-Fourier transforms.[10] The conjugate harmonic $Q(\phi)$ is finally formed by the sum of the two conjugate harmonics.
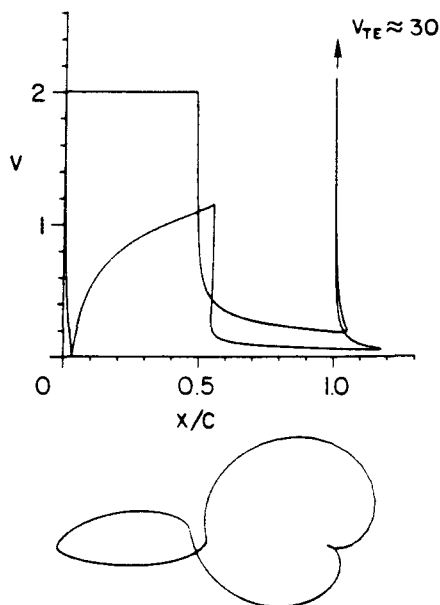


**Fig. 8 Example of a crossed airfoil with high trailing-edge velocity ratio ($\alpha = 15$ deg).**

### Multidimensional Newton Iteration

The condition that $P(\phi)$ satisfy the integral constraints, be continuous, and follow the special laws near the stagnation points is fundamental to the inverse airfoil design problem. In the design of any practical airfoil, however, more requirements are usually imposed. For example, the airfoil thickness ratio and pitching moment may be prescribed and the airfoil certainly must not cross over itself.

The pitching moment about the airfoil at zero lift is found from the Blasius theorem, which gives

$$c_{m_0} = \frac{4}{c^2} \int_0^{2\pi} P(\phi) \sin 2\phi \, d\phi \qquad (41)$$

This equation represents an additional integral constraint that $P(\phi)$ must satisfy for some specified value of the pitching moment coefficient. If the pitching moment is prescribed, the system of equations will include Eqs. (38), (39), and (41). Thus, an additional parameter must be relaxed to satisfy the system. In general, this must be done for each additional quantity prescribed.

Crossed airfoils are not excluded from the solution in any closed-form mathematical way. Figure 8, for example, shows a crossed airfoil with a cusped trailing edge and its velocity distribution at $\alpha = 15$ deg. Clearly, from the velocity distribution one could anticipate the resulting nonphysical airfoil. The problem stems from the large negative values of $K_H$ ($-12.62$) and $\bar{K}_H$ ($-16.64$), which give a high trailing-edge velocity ratio. Smaller values are needed to yield a trailing-edge velocity ratio on the order of that found for normal airfoil shapes, in particular, a velocity ratio less than unity. Iteration could be performed to yield a desired trailing-edge velocity ratio, but practical experience has shown that normal velocity distributions are usually obtained when the sum $K_H + \bar{K}_H$ is in the range 0 to 0.8—the smaller the sum in this range, the thinner the airfoil in the vicinity of the trailing edge. Thus, as in the Eppler method,[9,10]

$$K_S = K_H + \bar{K}_H \qquad (42)$$

serves as an equation to control the trailing-edge thickness distribution and is useful for preventing the occurrence of crossed airfoils.

In the present method, multidimensional Newton iteration is employed to solve the additional constraint equations [e.g., Eqs. (41) and (42)], which are now more appropriately termed the Newton equations. Quantities that are prescribed such as the airfoil thickness ratio and pitching moment represent the dependent Newton variables, and the additional unknowns necessary to satisfy the nonlinear system of equations represent the independent Newton variables. The independent Newton variables are selected from the parameters listed in Table 1. The iterative procedure begins with the solution of Eqs. (38) and (39), which determines $P(\phi)$ to define the airfoil velocity distribution. With $P(\phi)$, the dependent Newton variables are found by solving the necessary equations. Small perturbations are then sequentially added to the selected independent Newton variables, and the entire system is solved again for a new airfoil. From these perturbation solutions, the Jacobian of the Newton system is formed and used to predict the changes in the independent Newton variables needed to drive the airfoil design toward the desired goals. These changes are added to the independent Newton variables, and the process is repeated until the specified quantities are within a given tolerance of the desired values.

Conceptually, the iterative design procedure using multidimensional Newton iteration as outlined is not new. For supercritical cascade design, Sanz[18] iterated on input design parameters in the hodograph plane to control physical parameters of interest, specifically the entrance Mach number, inlet angle, turning angle, cascade solidity, and trailing-

edge gap. Although the design equations and solution formulation presented here and those of Sanz for supercritical cascade design are mathematically quite different, the two inverse approaches have much in common with respect to controlling parameters of interest through multidimensional Newton iteration.

### Examples of Newton Iteration in the Design Process

To demonstrate the capability of the Newton iteration procedure, an airfoil is to be designed such that $K_S = 0.5$ (to produce a normal trailing-edge shape), $c_{m_0} = -0.2$, and $t/c = 15\%$. The airfoil shown in Fig. 8 is used as the first guess in the Newton iteration procedure. Rather than attempting to satisfy all three design parameters at once, the design process is approached in stages that progressively attempt to satisfy the design constraints. Satisfying one or a few requirements per stage is favored because any arbitrary specifications may not correspond to a physical realizable airfoil. Moreover, going in stages often provides insight into potentially conflicting requirements and helps to determine which variables are best selected as the independent Newton variables. The airfoil of Fig. 8 is first uncrossed by iterating on the leading-edge arc limit $\phi_2$ to satisfy $K_S = 0.5$. This results in the airfoil shown in Fig. 9a. Next the velocity level $v_1$ and arc limit $\phi_2$ are iterated together to produce an airfoil with $K_S = 0.5$ and $c_{m_0} = -0.2$, as shown in Fig. 9b. In the last stage, $v_1$, $\phi_2$, and $\Delta\alpha^*$ are used as the independent Newton variables where the design angles of attack for the upper surface are replaced by $\alpha_1 + \Delta\alpha^*$ and $\alpha_2 + \Delta\alpha^*$ and for the lower surface by $\alpha_3 - \Delta\alpha^*$ and $\alpha_4 - \Delta\alpha^*$. The resulting airfoil with the three design parameters matched is shown in Fig. 10 along with the velocity distributions for $\alpha = 9.96$ and $5.04$ deg, the upper- and lower-surface design angles of attack.

The Newton iteration procedure is also employed to allow specification of the design velocity distribution in arc length $s$ and to locate a segment junction in $x/c$. In order to specify an $x/c$ location, for instance, at the beginning of the recovery, the corresponding arc limit is included as an independent Newton
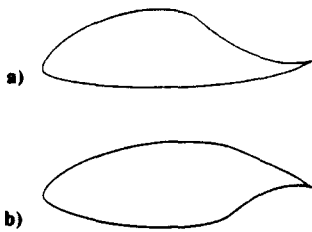
a)

b)
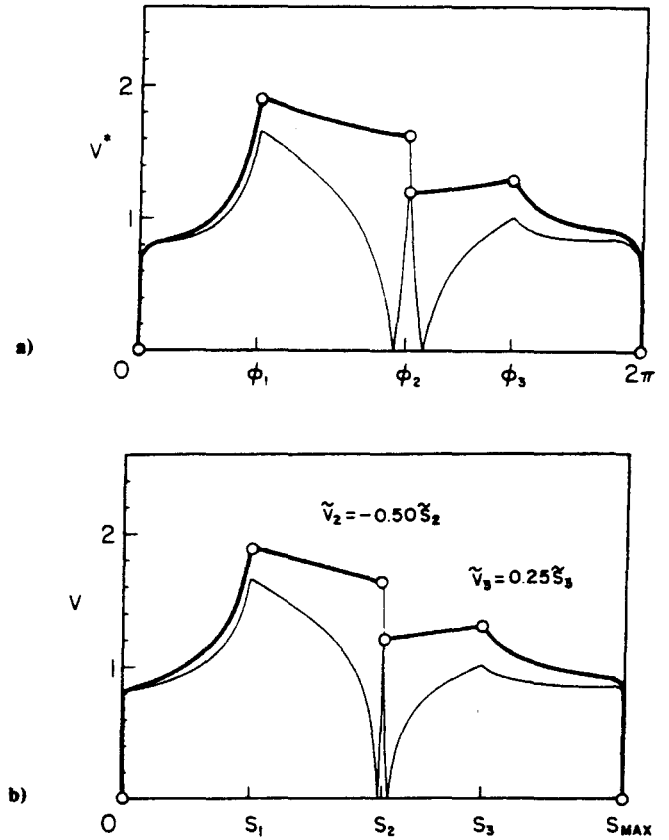
**Fig. 11** Velocity distributions at $\alpha = 1.19$ and $11.81$ deg as a function of a) $\phi$ and b) $s/c$.

variable. Specifying an arbitrary $v(s)$ for a segment would be inconsistent with the formulation of the problem as presented. Equations (39) determine the value of the velocity at the beginning of each segment so it cannot be prescribed (unless of course it is included for Newton iteration). Furthermore, the arc length along a segment is determined as part of the solution. It is not inconsistent, however, to prescribe the relative design velocity $\tilde{v}_i(\tilde{s}_i)$ subject to the condition $\tilde{v}_i(\tilde{s}_i = 0) = 0$ since $\tilde{v}_i(\tilde{\phi}_i = 0) = 0$. A desired distribution $\tilde{v}_i(\tilde{s}_i)$ is obtained through iteration on $\tilde{v}_i(\tilde{\phi}_i)$. The distribution $\tilde{v}_i(\tilde{s}_i)$ is satisfied at collocation points in $\tilde{\phi}_i$ for the particular segment, as indicated in Fig. 4. Each collocation point thereby gives rise to another equation in the Newton system.

Another example is presented to illustrate the capability of prescribing $\tilde{v}_i(\tilde{s}_i)$ and chordwise locations $x/c$. For the second and third segments, $\tilde{v}_2(\tilde{s}_2) = -0.50\tilde{s}_2$ and $\tilde{v}_3(\tilde{s}_3) = 0.25\tilde{s}_3$, respectively. The upper- and lower-surface recovery are prescribed to begin at 50 and 40% of chord, respectively. The airfoil is further constrained by specifying $c_{m_0} = -0.05$, $t/c = 25\%$, and $K_S = 0.3$. Lastly, the trailing-edge angle is specified to be 10 deg or $\epsilon = 1/18$. To meet these design goals, iteration is performed on the arc limits $\phi_1$, $\phi_2$, $\phi_3$, the velocity level $v_1$, the design angles of attack $\alpha_i$ through $\Delta\alpha^*$ (as previously described), and the relative design velocities $\tilde{v}_2(\tilde{\phi}_2)$ and $\tilde{v}_3(\tilde{\phi}_3)$. Figures 11a and 11b show the final velocity distributions at the resulting design angles of attack of 1.19 and 11.81 deg. For this airfoil, $\alpha_1 = \alpha_2$ and $\alpha_3 = \alpha_4$. As expected, the finite trailing-edge angle leads to zero velocity at the trailing edge. As depicted in Fig. 11b showing $v(s)$, the desired $\tilde{v}_i(\tilde{s}_i)$ for the second and third segments were achieved. Note that the arc length and relative arc lengths are normalized by the airfoil chord giving $s_{max}/c = 2.1$. The airfoil profile and velocity distributions in Fig. 12 show that the desired recovery locations are obtained. Finally, $c_{m_0}$, $t/c$, and $K_S$ also match the design specifications.

**Fig. 9** Airfoils produced by specifying a) $K_S = 0.5$, and b) $K_S = 0.5$, $c_{m_0} = -0.2$.
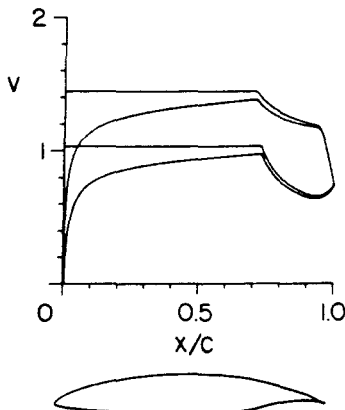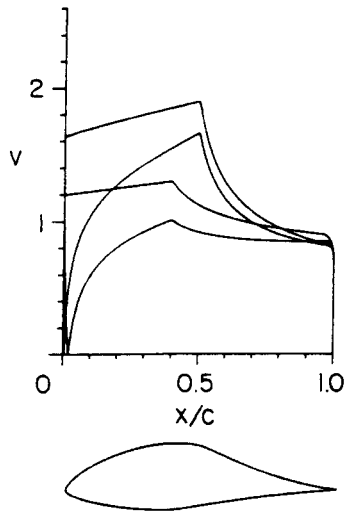
**Fig. 10** Airfoil with $K_S = 0.5$, $c_{m_0} = -0.2$, and $t/c = 15\%$ at $\alpha = 9.96$ and $5.04$ deg.

**Fig. 12   Airfoil and velocity distributions at $\alpha = 1.19$ and $11.81$ deg.**

Some remarks should be made regarding the choice of the independent Newton variables used to achieve the desired characteristics. In order for the design to resemble a normal airfoil and be uncrossed, $K_S$ is usually prescribed in the first stage of any new airfoil design. As employed in the examples, the leading-edge arc limit can usually be adjusted to drive $K_S$ to the desired value. Alternatively, the velocity level or any, all, or part of the design angles of attack may be adjusted. It is also possible to change the slope of $\bar{v}_i(\bar{\phi}_i)$ along a segment or several segments. Iteration for prescribed thickness or moment is usually successful through adjustments in the velocity level or design angles of attack. Several other options are available. Using $\bar{v}_i(\bar{\phi}_i)$ to achieve a given $\bar{v}_i(\bar{s}_i)$ is necessary. If a segment junction is to have a specified $x/c$ location, the corresponding segment arc limit must be iterated. As a final remark, if the specified design requirements are realistic, a group of independent Newton variables can usually be found.

## Concluding Remarks

Classically, inverse airfoil design is the problem of finding the airfoil shape given the desired velocity distribution. Aside from the extension to multipoint design with specification of global parameters, the present method is an example of such an approach. In addition to obtaining a desired velocity distribution, the designer often desires a particular boundary-layer development over part of the airfoil. In other cases, it may be desirable to control the geometry over a segment of the airfoil. Thus, a modern, general inverse airfoil design method should allow for specification of either the velocity distribution, boundary-layer development, or surface geometry along any given segment of the airfoil. Moreover, specification of global parameters should be permitted. The present formulation is a step in this direction. As a practical and versatile extension of the original theory of Eppler for multipoint inverse airfoil design, it allows for the prescription of a general velocity distribution over an arbitrary number of airfoil segments each at their respective design angles of attack. Thus, different parts of the airfoil can be designed specifically for different operating conditions. The example airfoils shown demonstrate the capabilities of the new method and the use of multidimen-

sional Newton iteration for obtaining desired airfoil characteristics not explicitly given as input to the inverse problem. In addition, the method is well suited to allow for specification of not only the desired velocity distribution but also for a prescribed boundary-layer development or surface geometry along any number of airfoil segments.

## References

[1]Lighthill, M. J., "A New Method of Two-Dimensional Aerodynamic Design," Aeronautical Research Council, R&M 2112, England, UK, April 1945.

[2]Glauert, M. B., "The Application of the Exact Method of Aerofoil Design," Aeronautical Research Council, R&M 2683, England, UK, Oct. 1947.

[3]Timman, R., "The Direct and Inverse Problem of Airfoil Theory. A Method to Obtain Numerical Solutions," National Aeronautical Research Inst., Rept. F.16, The Netherlands, 1951.

[4]Nonweiler, T. R. F., "A New Series of Low-Drag Aerofoils," Aeronautical Research Council, R&M 3618, England, UK, March 1968.

[5]Van Ingen, J. L., "A Program for Airfoil Section Design Utilizing Computer Graphics," AGARD-VKI Short Course on High Reynolds Number Subsonic Aerodynamics, AGARD LS-37-70, April 1969.

[6]Arlinger, G., "An Exact Method of Two-Dimensional Airfoil Design," Saab, TN 67, Linköping, Sweden, Oct. 1970.

[7]Strand, T., "Exact Method of Designing Airfoil with Given Velocity Distribution in Incompressible Flow," Journal of Aircraft, Vol. 10, No. 11, 1973, pp. 651–659.

[8]Eppler, R., " Direct Calculation of Airfoils from Pressure Distribution," NASA TT F-15, 417, March 1974. (Translated from Ingenieur-Archive, Vol. 25, No. 1, 1957, pp. 32–57.)

[9]Eppler, R., and Somers, D. M., "A Computer Program for the Design and Analysis of Low-Speed Airfoils," NASA TM-80210, Aug. 1980.

[10]Eppler, R., Airfoil Design and Data, Springer-Verlag, Berlin, 1990.

[11]Eppler, R., "Airfoil Program System, User's Guide," Institut A für Mechanik, University of Stuttgart, Stuttgart, Germany, March 1991.

[12]James, R. M., "A General Class of Airfoils Conformally Mapped from a Circle," McDonnell Douglas Corp., Rept. MDC-J5108, Long Beach, CA, 1971.

[13]Mangler, W., "Die Berechnung eines Tragflügelprofiles mit vorgeschriebener Druckverteilung," Jahrbuch der deutschen Luftfahrtforschung, Vol. 1, 1938, pp. 46–53; also, Air Ministry of London, Translation No. 932, 1940.

[14]Betz, A., "Änderung der Profilform zur Erzielung einer vorgegebenen Änderung der Druckverteilung," Luftfahrtforschung, Vol. 11, No. 6, Dec. 5, 1934, pp. 158–164; also, NACA Translation TM-767, 1935.

[15]Weinig, F., "Widerstands- und Tragflügelprofile mit vorgeschriebener Geschwindigkeitsverteilung an der Oberfläche," Zeitschrift für Angewählte Mathematik und Mechanik, Vol. 9, 1929, p. 507.

[16]Watson, E. J., "Formulæ for the Computation of the Functions Employed for Calculating the Velocity Distribution about a Given Aerofoil," Aeronautical Research Council, R&M 2176, England, UK, May 1945.

[17]Garrick, I. E., "Conformal Mapping in Aerodynamics, with Emphasis on the Method of Successive Conjugates," National Bureau of Standards Applied Mathematics Series 18: Constructions and Applications of Conformal Maps, U.S. Government Printing Office, Washington, DC, 1952.

[18]Sanz, M. J., "Automated Design of Controlled Diffusion Blades," American Society of Mechanical Engineers, Paper 88-GT-139, June 1988.